https://doi.org/10.5194/egusphere-2026-470
Preprint. Discussion started: 17 February 2026

Latent heat feedbacks and the self-lofting of seeded ice plumes: Insights from bin microphysics simulations

Huiying Zhang[1,★], Chia Rui Ong[2,★], Anurag Dipankar[2], Ulrike Lohmann[1], and Jan Henneberger[1]

[1]Institute for Atmospheric and Climate Science, ETH Zurich, Zurich, Switzerland
[2]Center for Climate System Modelling C2SM, ETH Zurich, Switzerland
★These authors contributed equally to this work.

Correspondence: Huiying Zhang (huiying.zhang@env.ethz.ch) and Chia Rui Ong (chiarui.ong@c2sm.ethz.ch)

Abstract. The interaction between environmental dynamics and microphysical processes governs the efficacy of glaciogenic cloud seeding, yet the extent to which initial vertical wind conditions dictate the evolution of seeded ice plumes remains poorly constrained. We investigate the dynamical and microphysical life cycle of ice plumes in supercooled stratiform clouds using idealized Large-Eddy Simulations (LES) coupled with the bin microphysics scheme SCALE-AMPS. Simulations of a targeted CLOUDLAB seeding experiment are constrained and validated by in situ observations. An ensemble of 20 simulations initialized with varying vertical wind velocities reveals a fundamental transition: while the initial trajectory is kinematically governed by the environmental vertical wind at cloud seeding, the long-term evolution is dominated by internal thermodynamic feedbacks. We identify a "self-lofting" mechanism wherein buoyancy generated by latent heat release from rapid ice growth overcomes initial subsidence, causing even downdraft-seeded plumes to eventually ascend. This thermodynamic response creates a structural trade-off: plumes initiated in updrafts are terminated by the cloud-top inversion, whereas those in downdrafts experience delayed ascent, resulting in a lager vertical dispersion. This expanded vertical extent compensates for the lower mean altitude of downdraft plumes, ensuring their geometrical detectability by downstream sampling in in observations. Microphysically, downdraft plumes undergo transient sublimation near cloud base but recover following buoyancy-driven re-ascent. These findings demonstrate that glaciogenic seeding is dynamically robust in low stratus clouds, as the seeded ice plume acts as an active thermodynamic agent capable of sustaining its residence time in the mixed-phase layer independent of the initial vertical wind state.

1 Introduction

Ice microphysical processes govern the phase partitioning, persistence, and radiative properties of mixed-phase clouds, thereby exerting a critical influence on Earth's hydrological cycle (Pruppacher et al., 1998; Korolev et al., 2017). These processes are intrinsically coupled to atmospheric dynamics: the interplay between vertical air motion, turbulence, and local supersaturation dictates ice crystal growth modes and cloud longevity (Korolev et al., 2003; Shupe et al., 2008). Vertical air motions are widely recognized as a primary driver of this evolution (Bühl et al., 2019; Shupe et al., 2008). Updrafts promote condensation and maintain liquid water by counteracting the Wegener–Bergeron–Findeisen (WBF) process — a mechanism wherein ice crystals

https://doi.org/10.5194/egusphere-2026-470
Preprint. Discussion started: 17 February 2026

grow at the expense of evaporating supercooled liquid droplets. In contrast, whereas downdrafts and subsidence favor glaciation and liquid water depletion (Rauber and Tokay, 1991; Korolev and Field, 2008; Bühl et al., 2019).

While vertical velocity fluctuations modulate ice nucleation efficiency and particle trajectories (Pinsky and Khain, 2002; Grabowski and Abade, 2017; Abade and Albuquerque, 2024), subsequent ice growth is accompanied by latent heat release. This thermodynamic response alters buoyancy and feeds back onto vertical motions, thereby further coupling microphysical and dynamical evolution (Morrison et al., 2012). However, the role of thermodynamic effects—particularly latent heat release associated with diffusional ice growth—in governing ice plume dynamics has received limited attention. A fundamental question therefore remains regarding the life cycle of ice in stratiform cloud layers: to what extent is the evolution of an ice plume determined by the vertical wind conditions at the time of ice initiation, as opposed to being shaped by subsequent microphysical–thermodynamic feedbacks?

Shallow mixed-phase clouds, such as stratocumulus and altocumulus, serve as an ideal natural laboratory for investigating these interactions. Compared to deep convection, these clouds are dynamically simpler, yet they exist in a thermodynamically metastable state where microphysical evolution is highly sensitive to the partitioning between liquid and ice phases (Ansmann et al., 2009; Westbrook and Illingworth, 2013). Glaciogenic cloud seeding offers a powerful framework for interrogating these systems by introducing a controlled source of ice crystals into supercooled clouds at a known time and location (CLOUDLAB, Henneberger et al. (2023)). Recent field campaigns employing uncrewed aerial vehicles (UAVs) and in situ instrumentation have enabled detailed characterization of seeded ice plumes, revealing rapid ice growth, efficient liquid water depletion, and enhanced aggregation (Miller et al., 2024, 2025; Ramelli et al., 2024; Fuchs et al., 2025; Zhang et al., 2025).

Nevertheless, such measurements are inherently Eulerian, providing snapshots of plume properties at fixed locations rather than a continuous record of their evolution. As a result, distinguishing whether the vertical transport of an ice plume is driven by the ambient vertical velocity into which it was born or by the buoyancy generated by its own growth remains difficult to establish from observations alone. Large-eddy simulations (LES) coupled with detailed bin microphysics schemes provide the necessary complementary tool to bridge this gap. Models such as SCALE–AMPS explicitly represent the size-, shape-, and habit-dependent evolution of ice particles while capturing the feedback between phase changes and air motion (Hashino and Tripoli, 2007b; Ong et al., 2022).

In this study, we use the SCALE–AMPS model to simulate a targeted seeding event from the CLOUDLAB campaign, utilizing in situ observations to constrain the initial conditions and validate the microphysical evolution. The paper is organized as follows. We first describe the experimental setup and the in situ dataset (section 2), followed by the numerical configuration of the SCALE–AMPS model (section 3). The model performance is then evaluated against observations by comparing key parameters such as Ice Crystal Number Concentration (ICNC), Liquid Water Content (LWC), and particle size distributions (subsection 4.1). Subsequently, we present the core sensitivity analysis, isolating the impact of initial vertical wind conditions on plume evolution and quantifying the role of latent heat feedbacks (subsection 4.2 and subsection 4.3). Finally, the main findings and their implications for future mixed-phase cloud studies are summarized (section 5).

https://doi.org/10.5194/egusphere-2026-470
Preprint. Discussion started: 17 February 2026

2 Observational Setup and Data

This study focuses on a single glaciogenic seeding experiment from the CLOUDLAB campaign in persistent wintertime supercooled stratus over the Swiss Plateau near Eriswil, Switzerland (47°04′14″N, 7°52′22″E; 920 m a.s.l.) (Scherrer and Appenzeller, 2014; Henneberger et al., 2023; Miller et al., 2024, 2025; Ramelli et al., 2024; Fuchs et al., 2025). The experiment was conducted on 24 January 2023 at 18:08:57 UTC in liquid-dominated, quasi-stationary cloud conditions with temperatures close to $-5\,^{\circ}\mathrm{C}$ at seeding height. Glaciogenic seeding was performed at an altitude of 1348 m, 2068 m upwind of the measurement site, under mean wind directions between 75° and 77°. As the seeded ice plume advected over a fixed ground-based site, its microphysical changes were continuously sampled by an in situ platform, providing time-resolved observations used both to constrain the model setup and to evaluate the simulated ice growth and interaction processes. The sampling altitude during plume observation was generally consistent with the seeding height, with vertical fluctuations of up to about ± 30 m.

In situ measurements were obtained using a tethered balloon system carrying the HOLographic Imager for Microscopic Observations (HOLIMO; Ramelli et al. 2020), a digital in-line holography instrument with effective spatial resolutions of 6 µm for cloud droplets and 25 µm for ice crystals. Holograms were reconstructed, and detected particles were initially classified using a convolutional neural network (Touloupas et al., 2020). Ice crystals classified by this procedure were subsequently analyzed using IceDetectNet-CLOUDLAB (Zhang et al., 2025), a CLOUDLAB-specific fine-tuning of IceDetectNet (Zhang et al., 2024). The uncertainty in cloud droplet number concentration is approximately 5 %, while uncertainties in ice crystal number concentration range from 5–10 % for larger crystals and increase to about 15 % for smaller particles.

The numerical simulation is configured to reproduce this experiment using observationally constrained initial and environmental conditions as follows: The model is initialized with a liquid water path of 107.5 g m^{-2} measured from HATPRO Microwave Radiometer. Thermodynamic profiles for the model setup are derived from radiosonde launches at 15:44, 20:31, and 20:48 UTC on 24 January 2023, which span the seeding and plume observation period. Model performance is evaluated against the observed ice size distribution, aspect ratio, ICNC, CDNC, LWC, and inferred collision rate, using consistent definitions and averaging procedures for model output and observations.

3 Method

3.1 Model

The SCALE-AMPS model (Nishizawa et al., 2015; Sato et al., 2015; Ong et al., 2022) is used in this study. SCALE is a large-eddy simulation (LES) atmospheric model that solves the primitive equations using the finite-volume formulation on a structured Arakawa C-staggered grid. Prognostic variables are advanced in time using the fourth-order Runge–Kutta integration scheme. Subgrid-scale turbulence is represented using a Smagorinsky–Lilly–type scheme (Smagorinsky, 1963; Lilly, 1962), and radiative transfer is computed with the MSTRNX radiation code (Sekiguchi and Nakajima, 2008).

AMPS is a habit-preserving bin microphysics scheme. Detailed descriptions of AMPS are provided in Hashino and Tripoli (2007b, 2008, 2011), and its implementation within the SCALE framework is described by Ong et al. (2022). Here, only a brief

https://doi.org/10.5194/egusphere-2026-470
Preprint. Discussion started: 17 February 2026

overview is given. Both liquid and ice particle size spectra are discretized into 40 bins. For each liquid bin, tracer variables include the liquid water mixing ratio (Qliq), Cloud Droplet Number Concentration (CDNC), aerosol mixing ratio (Qae), and the mean ratio of soluble mass to total aerosol mass (Qsolv). For each ice bin, the corresponding variables are the ice mixing ratio (Qice), ICNC, Qae, and Qsolv.

To keep track of the evolution of the shape of ice particles, three additional tracer variables corresponding to the a-axis and c-axis lengths are stored in each ice bin. These variables allow the model to keep track of the time evolution of habit changes, as ice particles grow into different shapes (e.g., planar or columnar) depending on ambient temperature. Aggregation (Qagg) and riming (Qrim) mixing ratios are also predicted, because collisions with ice particles and liquid droplets alter particle mass compositions and shapes. AMPS assumes that aggregation and riming processes cause ice particles to asymptotically approach an elliptical shape. A third mass-component prognostic variable, the crystal mass mixing ratio (Qcry), is included to track the history of vapor deposition growth. Vapor deposition growth increases only Qcry, while Qagg and Qrim remain unchanged. For pristine ice particles that grow exclusively by vapor deposition, Qcry = Qice within a bin.

A cubic polynomial is used to represent the subgrid-scale distribution of number density in both the liquid and ice spectra. During diffusional or collisional growth, particle mass changes cause the lower and upper boundaries of a bin to shift. The subgrid distribution in each shifted bin is recalculated, and the prognostic variables in the original bins are updated by integrating the corresponding quantities over the overlapping regions between the shifted and original bins. The ratios Qcry/Qice, Qagg/Qice and Qrim/Qice are assumed to remain constant within the subgrid distribution. This is a strategy called implicit mass sorting assumption (Hashino and Tripoli, 2007b). When two ice particles collide, the post-collision axis lengths are computed using the volumetric means.

The relative growth rates of the a- and c-axis lengths are determined by an inherent growth-rate function that depends solely on ambient temperature (Chen and Lamb, 1994). AMPS uses a single spectrum for all types of ice particles. Ice particle types can be diagnosed within each bin based on the crystal, aggregation and riming mass fractions (Qcry/Qice, Qagg/Qice, and Qrim/Qice). In AMPS, ice particles are classified as one of the following types: pristine crystals, rimed crystals, graupel, aggregates, or rimed aggregates (Hashino and Tripoli, 2007a). For example, ice particles are diagnosed as aggregates when the aggregation mass fraction exceeds 10% and the riming mass fraction is less than 10%.

Cloud condensation nuclei (CCN) are treated as a spatially uniform background variable throughout this study and are assumed to follow a lognormal size distribution. The distribution is discretized into 10 bins in the computation of CCN activation. CCN in bins with critical supersaturations lower than the ambient supersaturation are activated and transferred to the liquid water bins, with the resulting droplet size and bin assignment determined by the microphysics time step and the initial droplet growth rate. Activated CCN are immediately replenished to maintain the prescribed background distribution.

3.2 Numerical setup

The computational domain spans 2 km and 4 km in the x and y directions, respectively, with the model top at 1 km. The grid spacing is uniformly 20 m in the x, y, and z directions. Periodic boundary conditions are applied in the horizontal directions, and Rayleigh damping is imposed above 800 m. Complex orography over the Swiss Plateau at the field campaign site is not

https://doi.org/10.5194/egusphere-2026-470
Preprint. Discussion started: 17 February 2026

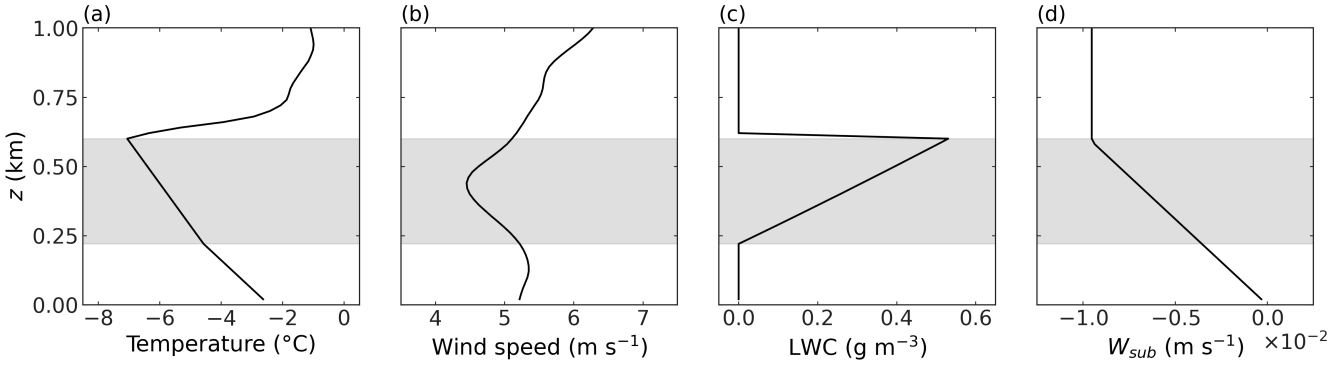

Figure 1. Vertical profiles of (a) temperature, (b) wind speed, and (c) liquid water content (LWC) used as the initial conditions for the simulations. The mean wind is directed in the positive y direction. Panel (d) shows the imposed large-scale subsidence W_{sub}. The gray shaded region denotes the cloud layer.

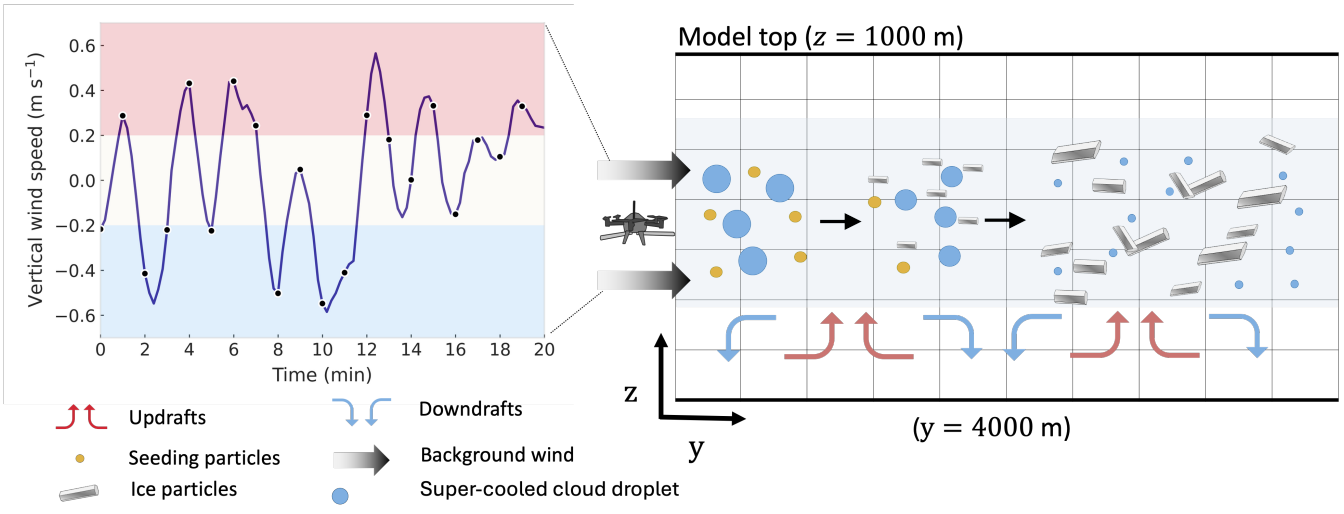

Figure 2. One-minute running average of the vertical wind speed in the grid cells where ice-nucleating particles (INPs) are released, and (b) schematic illustration of the computational domain after the spin-up period. Cloud seeding is performed between the coordinates (950, 10, 310) and (1050, 10, 310) m.

represented; consequently, the domain is flat. This idealization may lead to an underestimation of turbulent mixing associated with real terrain. The cloud layer extends from approximately 220 to 600 m in altitude. Accordingly, the relative humidity is
125 prescribed as 100% within this layer and varies linearly below and above the cloud, with boundary conditions derived from radiosonde observations. The initial vertical profiles of temperature and liquid water content (LWC; Fig. 1) are derived from the linearized relative humidity profile, observed pressure, and the assumption of a vertically uniform liquid potential temperature below cloud top. The initial wind profile is obtained by smoothing the radiosonde observations, with the mean flow oriented in

https://doi.org/10.5194/egusphere-2026-470
Preprint. Discussion started: 17 February 2026

the y direction. In all simulations, the wind speed is nudged toward the initial profile with a relaxation time scale of 1 h. Model output is saved at 12-s intervals.

A constant large-scale subsidence of 0.00952 m s^{-1} (Fig. 1d) is imposed above the inversion layer at 600 m above ground to maintain a steady boundary layer depth and inversion strength throughout the simulations, as the simulations are idealized and do not include realistic boundary conditions. The subsidence is assumed to be zero at the surface and is linearly interpolated at altitudes between the inversion layer and the surface. Its effect on temperature and water vapor mixing ratio is represented by adding a source term $-w\partial\phi/\partial z$ in the energy and moisture equations, where w is the subsidence and ϕ denotes temperature or water vapor mixing ratio, to their respective prognostic tendencies.

Observational constraints on the physical and chemical properties of background CCN are unavailable. We therefore assume that the CCN consist entirely of ammonium bisulfate, with a mean particle radius of 0.052 μm and standard deviation of the CCN size distribution of 0.071. The observed mean cloud droplet number concentration is 317 cm^{-3}; accordingly, the background CCN number concentration is prescribed as 317 cm^{-3}.

The first hour of integration is treated as a spin-up period to allow the model to adjust dynamically and thermodynamically to the imposed initial and boundary conditions. A spin-up time of 1 h is sufficient for turbulent flows in the boundary layer to fully develop and for the mean liquid water path and CDNC to approach quasi-steady values (not shown). After the spin-up period, a series of updrafts and downdrafts emerges within the boundary layer (see the schematic illustration of the idealized simulation setup in Fig. 2). These motions are generated by thermal convection in the presence of wind shear and surface friction. They propagate downstream and evolve with time, with existing updrafts and downdrafts dissipating and new ones forming. Their vertical extent can reach the cloud top.

Ice-nucleating particles (INPs) are released for 1 min at a uniform rate of 10 cm^{-3} s^{-1} within grid cells spanning the coordinates (950, 10, 310) to (1050, 10, 310) m, where the three indices denote the x, y, and z coordinates, respectively. The injection altitude is chosen to match the actual seeding altitude, at which the ambient air temperature upon seeding is -5 °C. Ice particles form from the injected INPs and are subsequently advected downstream by the mean wind.

The freezing efficiency of INPs is parameterized following Omanovic et al. (2024), with the frozen fraction defined as

$$\mathrm{F_{ice}} = \frac{-b}{1+\exp(-k(T-T_0))} + b \tag{1}$$

where $\mathrm{F_{ice}}$ is the frozen fraction, T is temperature (K), $b = 0.97$, $k = 0.88$, and $T_0 = 263.95$ K. New ice particles form when $\mathrm{F_{ice}N_{INP}}$, where $\mathrm{N_{INP}}$ is the total INP number concentration in a grid cell, exceeds the existing ICNC. All INPs are assumed to have a uniform diameter of 1.0 μm and are treated as passive tracers. Consequently, they do not interact dynamically with the flow, and their chemical composition and mass are not explicitly represented.

After the spin-up period, the 1-min running mean vertical wind speed within the seeding grid cells fluctuates between -0.6 and 0.6 m s^{-1} (left panel of Fig. 2). To investigate the sensitivity of the ice plume evolution to vertical wind speed, we perform 20 seeding simulations, with the initiation time of INP release staggered at 1-min intervals. The simulation in which INPs are released 9 min after the spin-up period is selected as the reference case, and its results are compared with observational data to evaluate the validity of the model and the numerical setup. The 20 simulations are categorized into three groups: (1) updraft,

https://doi.org/10.5194/egusphere-2026-470
Preprint. Discussion started: 17 February 2026

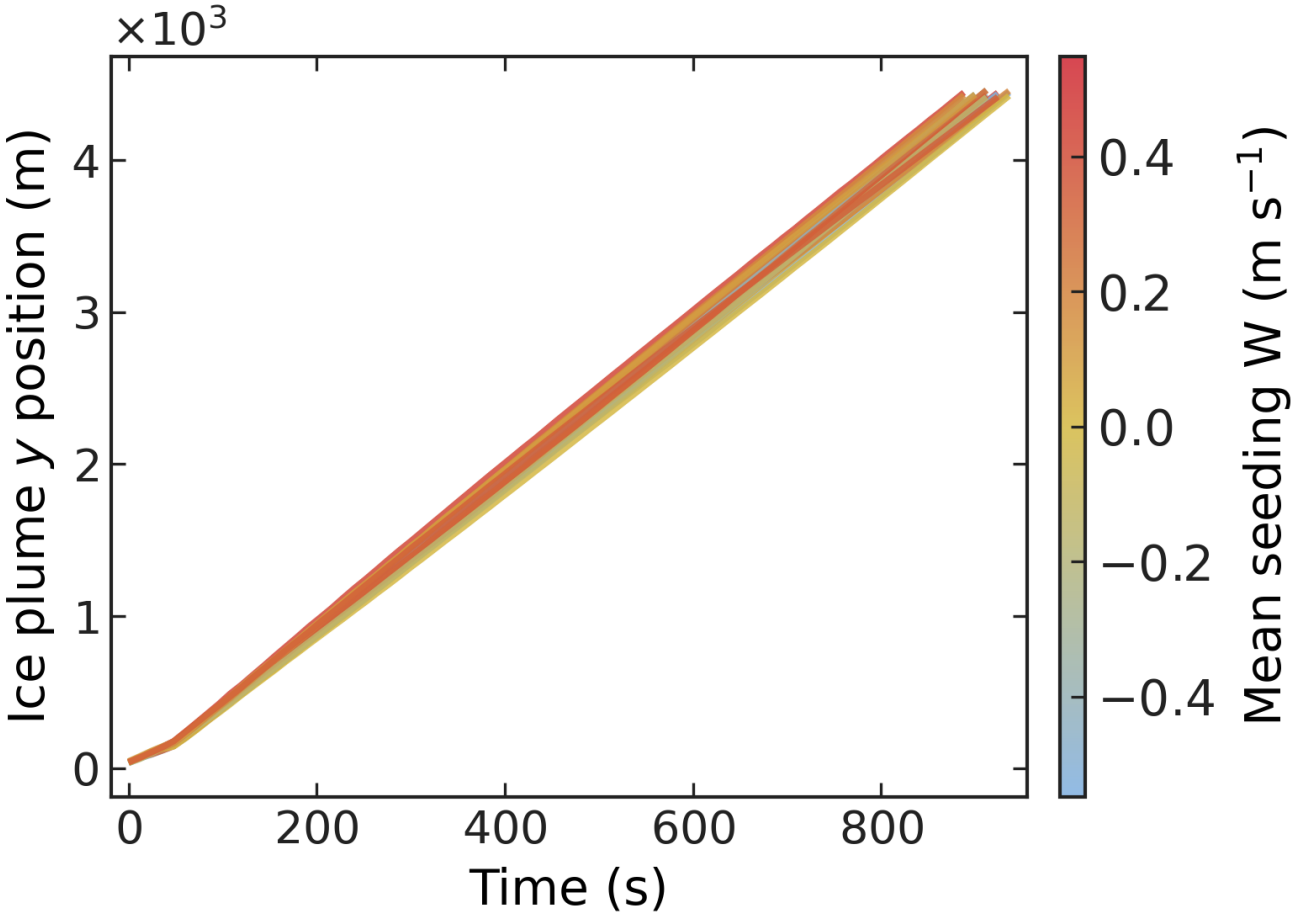

Figure 3. Time series of the downstream distance (y position) advected by the ice plume for all simulations.

(2) no-wind, and (3) downdraft, based on the mean vertical wind speed at the seeding location greater than 0.2 m s^{-1}, between -0.2 and 0.2 m s^{-1}, and less than -0.2 m s^{-1}, respectively. This classification yields 7 updraft, 6 no-wind, and 7 downdraft simulations. For the sensitivity analysis, the ice plume is defined as the set of grid cells in which the ICNC exceeds the 70th percentile.

The mean wind speed in the y direction exhibits weaker variability than the initial profile by the end of the spin-up period, as the boundary layer becomes well mixed by convection and turbulence. The wind speed decreases only slightly from approximately 5.1 m s^{-1} near the surface to 4.8 m s^{-1} near the cloud top. Consequently, the ice plume in all simulations advects downstream at an approximately constant speed in the y direction (Fig. 3). In the reference simulation, the ice plume travels 2 km in 444 s. The time required for the ice plume to travel 4 km varies between 804 and 852 s among the simulations.

https://doi.org/10.5194/egusphere-2026-470
Preprint. Discussion started: 17 February 2026

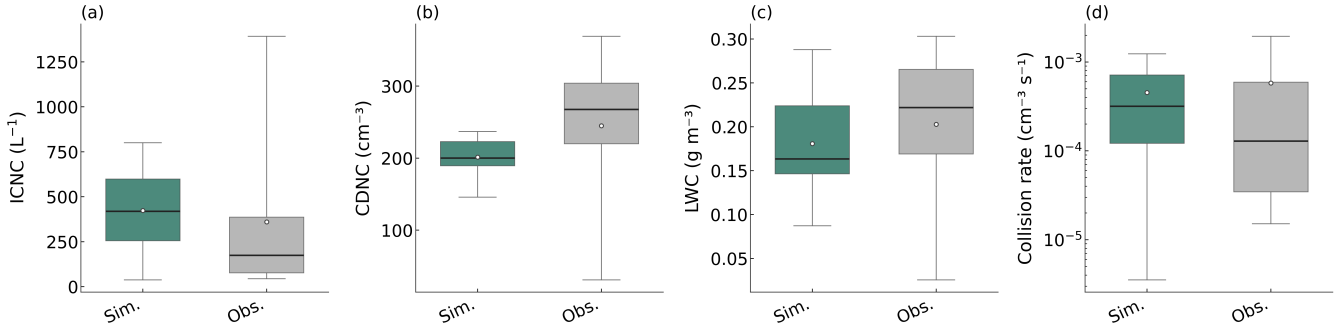

Figure 4. Simulated and observed (a) ICNC, (b) CDNC, (c) LWC, and (d) collision rate at 2 km downstream of the seeding location. The simulation results are sampled at the height between 400 and 450 m above ground, while the observational data are taken at 400 m above ground.

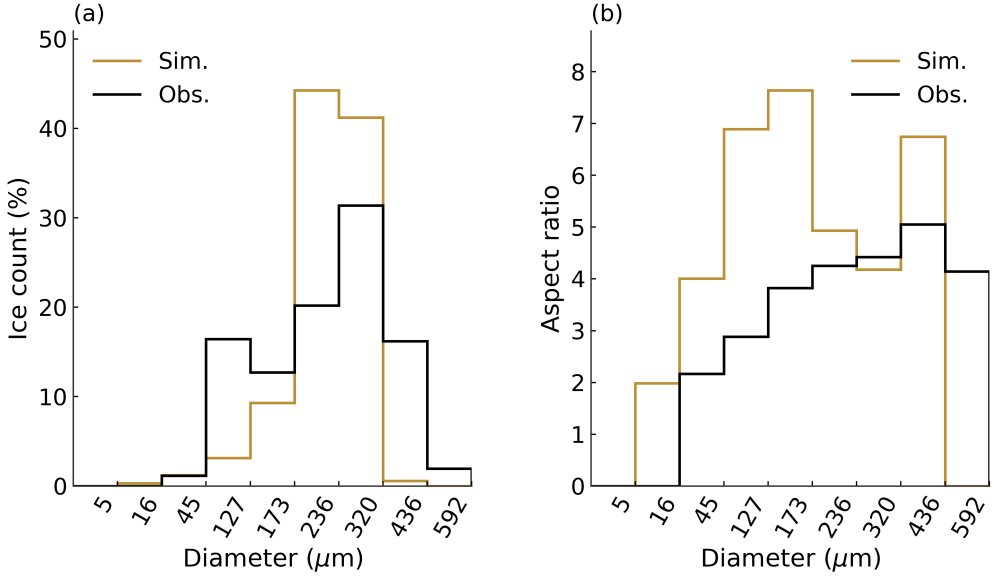

Figure 5. Simulated and observed (a) ice count and (b) aspect-ratio distributions at 2 km downstream of the seeding location.

4 Results

4.1 Model validation

In this section, the validity of the numerical setup is assessed by comparing results from the reference simulation with in situ observations obtained on 24 January 2023. Specifically, comparisons are made for ICNC, CDNC, liquid water content (LWC) particle aspect ratio, and ice particle size distribution. In the simulation, these quantities are sampled in grid cells located 2 km downstream of the seeding region, between height of 400 and 450 m above ground, when the ice plume passes through and

https://doi.org/10.5194/egusphere-2026-470
Preprint. Discussion started: 17 February 2026

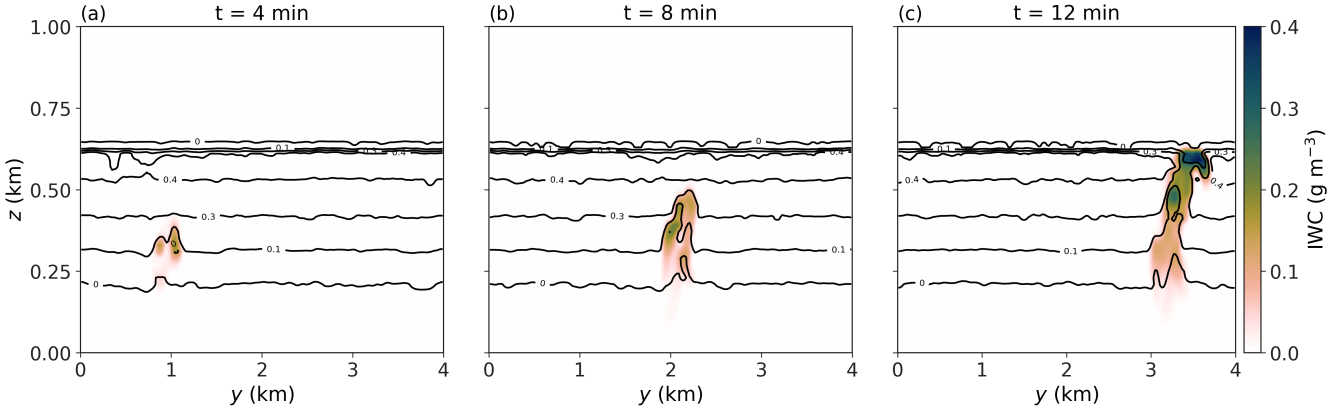

Figure 6. IWC and LWC (contour lines) at x = 2000 m at 4, 8, and 12 min after seeding begins.

ICNC exceeds 10 L^{-1}. This sampling strategy is designed to match the location of the observational measurements, which were collected at approximately 400 m above ground level (AGL) and 2 km downstream from the seeding drone.

The simulated mean values of ICNC, CDNC, LWC, and collision rate agree reasonably well with the observed means (Fig. 4) considering that the set up is idealized. Although the simulated median CDNC and LWC are approximately 70 cm^{-3} and 0.05 g m^{-3} lower than the observed medians, owing to a higher simulated median ICNC, the interquartile range (25th-75th percentiles) of the simulated LWC lies within the range of the observed LWC. The observational data exhibit greater variability than the simulation. This discrepancy may be attributed to three factors: (1) small-scale inhomogeneity that is not fully resolved by the grid spacing used in the simulation; (2) the idealized setup, which employs smoothed initial conditions and neglects the complex terrain.

In the simulation, ice particles grow predominantly by vapor deposition. Consequently, the simulated size distribution is narrower than that observed (Fig. 5). Most simulated particles have sizes between 173 and 320 μm, whereas the observed size distribution peaks between 236 and 320 μm. This difference is also likely due to the absence of turbulent effects that would otherwise broaden the particle size distribution (Grabowski and Abade, 2017), as well as insufficient spatial inhomogeneity.

For particles with sizes between 173 and 320 μm, the simulated mean aspect ratio ranges from 4 to 5, in good agreement with observed values (Fig. 5). However, the simulated mean aspect ratio of ice particles smaller than 173 μm reaches approximately 7. This bias arises because some ice particles form at colder temperatures after the ice plume ascends to higher altitudes. Over this temperature range in the boundary layer, the aspect ratio (c-axis/a-axis) increases more rapidly at colder temperatures (Chen and Lamb, 1994), leading to larger aspect ratios for particles formed later in the plume evolution.

The ice plume initially appears as a localized feature, with a horizontal extent of approximately 300 m and a top height near 400 m 4 min after INPs are released into the computational domain (Fig. 6). After traveling 2 km downstream, the plume top reaches an height of about 500 m above ground, while its horizontal extent remains nearly unchanged. The vertical extent of the ice plume continues to increase with time, and it eventually spans the entire cloud depth at 3 km downstream.

https://doi.org/10.5194/egusphere-2026-470
Preprint. Discussion started: 17 February 2026

Overall, although the simulated ice plume exhibits greater spatial homogeneity and potentially weaker turbulent effects than observed, the model is able to reproduce the key mean characteristics of the ice plume. Good agreement is achieved between the reference simulation and observations in terms of mean ICNC, CDNC, LWC, collision rate, ice particle size, and aspect ratio. This numerical configuration therefore provides a foundation for the subsequent sensitivity experiments investigating the influence of vertical velocity at the seeding location.

4.2 Latent heat feedbacks and vertical plume dispersion

The vertical trajectory of the seeded ice plume is initially kinematically governed by the environmental vertical wind field at the point of injection. As illustrated in Fig. 7(a), plumes injected into updraft regions undergo rapid ascent, reaching the cloud-top height ($z \approx 600$ m above ground) within 6 to 10 minutes. Conversely, plumes seeded into subsiding air parcels ($w_{init} < 0$) experience an initial loss of altitude, descending by up to 150 m within the first 300 seconds. However, a fundamental dynamic transition is observed as the plume evolves: the trajectory decouples from the initial environmental forcing, and all plumes eventually establish a coherent net ascent. Even simulations initialized in strong downdrafts reverse their vertical motion, initiating a secondary ascent phase after approximately 300 to 500 seconds.

We hypothesize that this unconditional lofting is driven by internal microphysical–thermodynamic feedbacks, specifically the buoyancy generated by the latent heat of phase changes. The rapid growth of seeded ice crystals—primarily through vapor deposition in the supersaturated mixed-phase environment—releases a significant amount of latent heat. This exothermic process induces a localized positive temperature perturbation within the plume relative to the environment, thereby generating buoyancy that opposes and eventually overcomes the initial downdraft momentum.

This mechanism is quantitatively substantiated by two lines of evidence. First, the mean vertical velocity (W) within the plume converges towards positive values across the entire ensemble, independent of the initial kinematic state (Fig. 7b). Second, and more critically, there is a robust functional relationship between the seeding-induced vertical velocity perturbation (ΔW) and the cumulative latent heat release ($Q - Q_{no\_ice}$), as shown in Fig. 7(c). The increase of ΔW with accumulated heat confirms that the secondary updraft is not a stochastic feature of the turbulence but a deterministic response to the latent heat released upon phase changes.

The interaction between this buoyancy-driven ascent and the thermodynamic stability at the cloud top (the capping inversion) fundamentally alters the vertical morphology of the plume. Plumes in updrafts possess high vertical momentum and reach the inversion layer rapidly (short residence time in the boundary layer). Upon impact, their ascent is stopped, causing the plume to spread horizontally (see Appendix „„). In contrast, plumes in downdrafts exhibit a delayed ascent and a longer residence time within the mixed-phase layer. This extended transit allows for greater vertical dispersion before reaching the ceiling. Consequently, as evidenced in Fig. 8, downdraft-seeded cases cause a significantly larger vertical spread (up to ~ 250 m) at downstream distances compared to the vertically constrained updraft cases.

These dynamical differences have critical implications for the observational verification of the seeding signal. The in-situ measurement sampling was conducted at a downstream distance corresponding to an advection time of $t \approx 464$ s, at an altitude proximate to the seeding level. At this temporal snapshot (Fig. 8a), a significant vertical bifurcation is evident: while the

https://doi.org/10.5194/egusphere-2026-470
Preprint. Discussion started: 17 February 2026

centroids of the updraft-seeded plumes have ascended well above the sampling height (exceeding 500 m above ground), the downdraft-seeded plumes remain low, with centroids as low as ~ 150 m. However, the enhanced vertical dispersion in the downdraft regime plays a critical compensatory role. These plumes occupy a much deeper vertical column, with a vertical extent reaching up to ~ 250 m (Fig. 8 (a)). This expanded vertical geometry ensures that even when the plume center of mass is below the flight level, the upper parts of the plume likely intersect the sampling height. Furthermore, this structural characteristic persists further downstream, as evidenced by the consistent spread statistics at $y = 3$ km and $y = 4$ km (Fig. 8b, c). Consequently, despite the substantial variability in initial vertical trajectories, the seeding signature remains robustly detectable, as the thermodynamic feedbacks effectively broaden the spatial probability of interception.

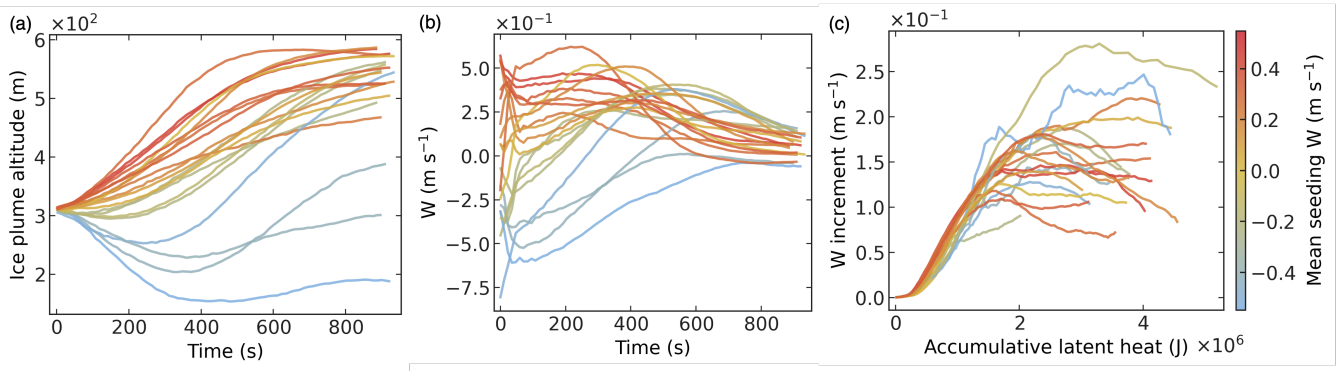

Figure 7. Temporal evolution of ice plume dynamics and thermodynamic feedbacks. (a) Mean altitude of the ice plume center of mass. The observational sampling time corresponds to $t \approx 464$ s. (b) Evolution of the mean vertical wind speed (W) within the ice plume. (c) The relationship between the seeding-induced vertical velocity perturbation (ΔW) and the accumulative latent heat release. The strong positive correlation confirms that latent heating drives the secondary ascent.

4.3 Microphysical evolution of the ice plume

The properties of the trajectories discussed in Sect. 4.2 influence the microphysical evolution of the seeded plume. Figure 9 presents the temporal evolution of the bulk ice properties. ICNC exhibits a rapid, monotonic decay across all simulations (Fig. 9a), driven primarily by turbulent dispersion and dilution rather than aggregation or sedimentation loss. While the decay rates are generally comparable, the downdraft-seeded plumes (blue lines) display a slightly more pronounced reduction in ICNC between $t = 100$ and 400 s compared to updraft and no-wind cases. This aligns with the findings in Fig. 8, where downdraft plumes undergo greater vertical expansion, leading to stronger volumetric dilution. However, by $t = 800$ s, ICNC values across all regimes converge, suggesting that dispersion eventually homogenizes the number density regardless of the initial perturbation.

In contrast to the convergence of number concentration, the evolution of ice particle size and mass shows significant divergence based on the vertical wind regime. The mean ice diameter (D_{ice}, Fig. 9b) increases continuously due to vapor deposition. Plumes in updrafts develop the largest crystals, followed by no-wind and downdraft cases. This stratification is even more dis-

https://doi.org/10.5194/egusphere-2026-470
Preprint. Discussion started: 17 February 2026

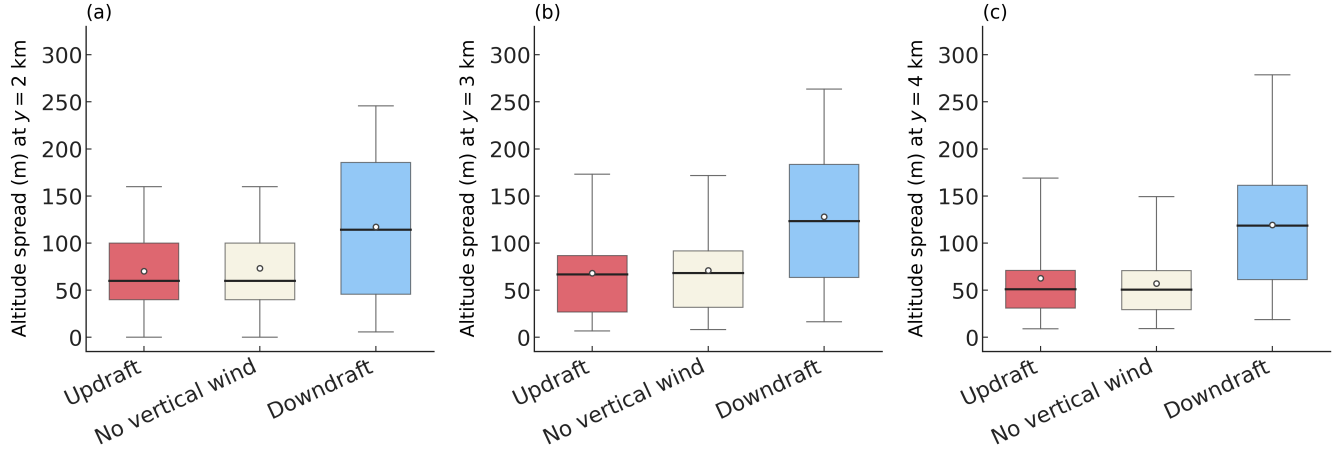

Figure 8. Boxplots of the vertical extent (altitude spread) of the ice plumes sampled at downstream distances of (a) $y = 2$ km, (b) $y = 3$ km, and (c) $y = 4$ km. Simulations are categorized by the vertical wind conditions at the injection time: Updraft ($w_{init} > 0.2$ m s^{-1}), No vertical wind ($-0.2 \leq w_{init} \leq 0.2$ m s^{-1}), and Downdraft ($w_{init} < -0.2$ m s^{-1}).

tinct in the Ice Water Content (IWC, Fig. 9c). The updraft plumes, which are lofted rapidly into the supersaturated upper cloud regions, experience optimal growth conditions, resulting in the highest IWC. Conversely, downdraft plumes, which initially subside towards the cloud base or into sub-saturated air, experience suppressed growth rates, yielding significantly lower ice mass despite having similar number concentrations.

The evolution of the size distribution of the ice crystals confirms that while the growth rate varies, the growth mode remains consistent. Figure 10 displays the Particle Size Distributions (PSD) at downstream distances of $y = 2, 3$, and 4 km. Across all wind conditions, the PSDs exhibit a coherent rightward shift (towards larger diameters) over time. The structural similarity of the PSD among the three regimes suggests that the seeding mechanism determines the initial spectral characteristics, while the environmental vertical velocity primarily modulates the rate of the size shift rather than altering the fundamental shape of the distribution.

The growth of ice occurs at the expense of the liquid phase via the WBF process. This interaction is evident in Fig. 11, where CDNC decreases as the plume evolves. An anomaly is observed in the downdraft and no-wind simulations around $t \approx 200$ s: both CDNC (Fig. 11a) and mean liquid diameter (D_{liq}, Fig. 11b) exhibit a sharp minimum, coinciding with a drop in Relative Humidity (RH) (Fig. 11c). This "dip" corresponds to the period when subsiding plumes approach or penetrate cloud base, encountering drier air and causing partial evaporation or rapid glaciation. As the secondary lofting mechanism (driven by latent heat) takes over after $t > 300$ s, the plumes re-ascend into the mixed-phase layer, allowing RH and liquid properties to stabilize. This highlights that seeding into downdrafts carries a risk of transient sublimation, although the plume ultimately recovers.

https://doi.org/10.5194/egusphere-2026-470
Preprint. Discussion started: 17 February 2026

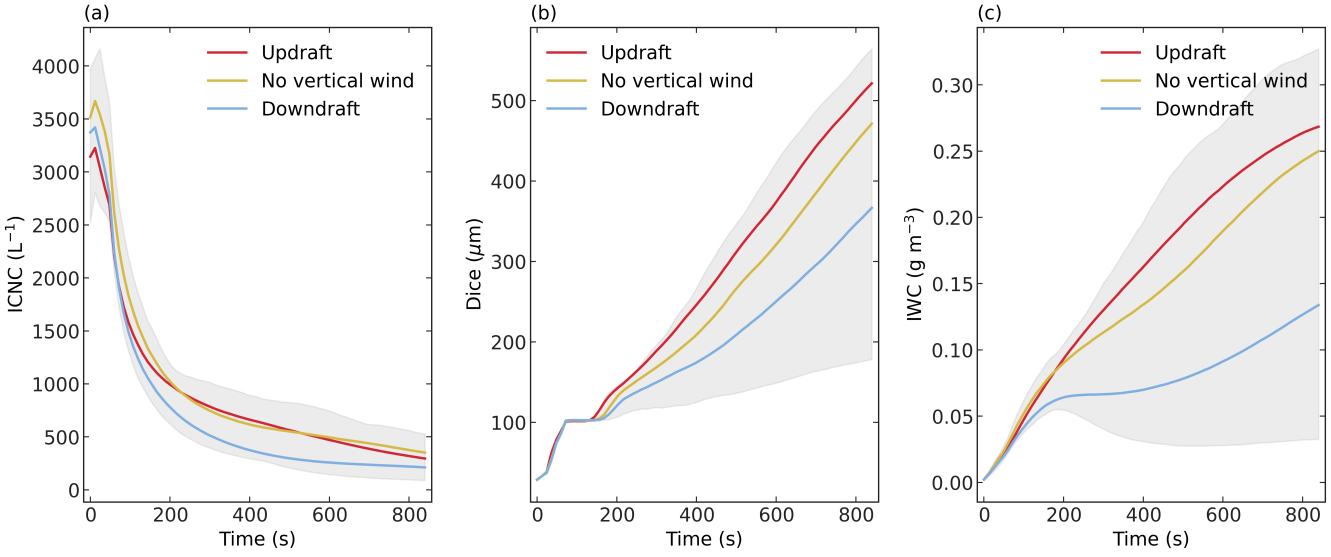

Figure 9. Temporal evolution of mean ice microphysical properties averaged within the plume. (a) Ice Crystal Number Concentration (ICNC), showing dilution due to dispersion. (b) Mean ice diameter (D_{ice}). (c) Ice Water Content (IWC). Shaded areas represent the standard deviation across the ensemble members for each wind regime.

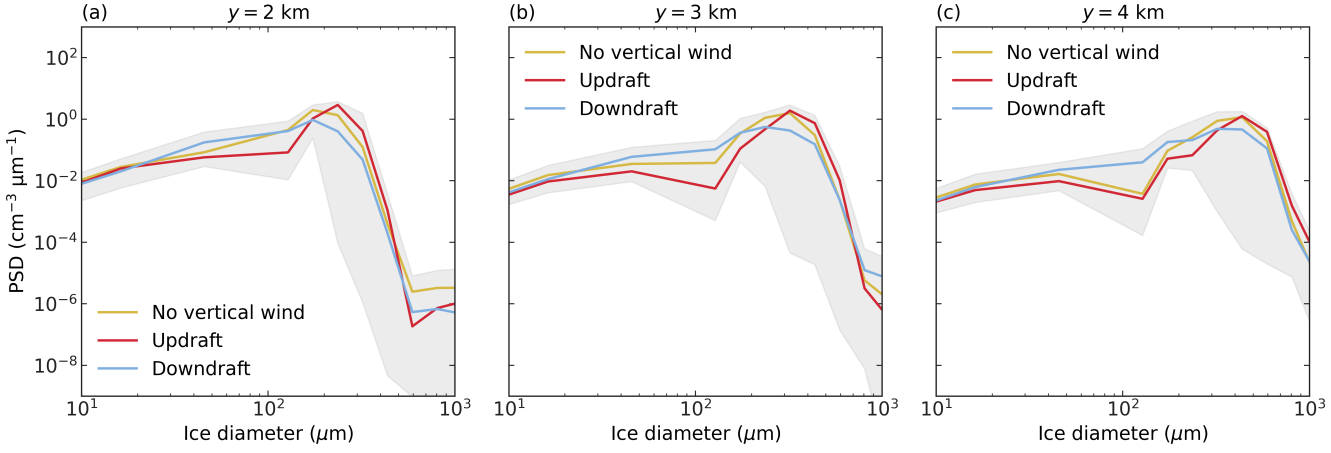

Figure 10. Evolution of Ice Particle Size Distributions (PSD) sampled at downstream distances of (a) $y = 2$ km, (b) $y = 3$ km, and (c) $y = 4$ km.

5 Conclusions and outlook

In this study, we investigated the dynamical and microphysical life cycle of glaciogenic ice plumes in supercooled stratiform clouds using the detailed bin microphysics model SCALE-AMPS. By constraining the simulations with in situ observations

https://doi.org/10.5194/egusphere-2026-470
Preprint. Discussion started: 17 February 2026

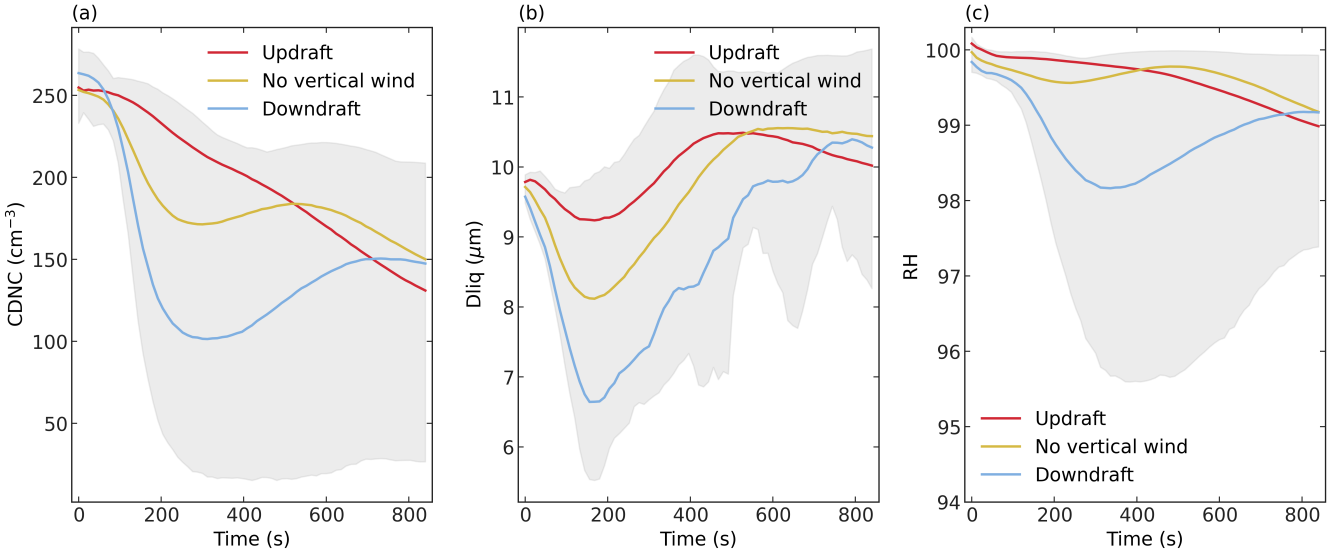

Figure 11. Temporal response of the liquid phase within the ice plume. (a) Cloud Droplet Number Concentration (CDNC). (b) Mean liquid droplet diameter (D_{liq}). (c) Relative Humidity (RH) with respect to water.

from the CLOUDLAB campaign, we successfully reproduced key plume characteristics—including ice number concentration, liquid water depletion, and particle size distributions—thereby establishing a robust framework for isolating the impact of environmental vertical wind conditions on seeding efficacy.

Our sensitivity analysis reveals that the evolution of a seeded ice plume is not merely a passive response to the initial advective field but is fundamentally shaped by latent heat release. The key findings are summarized as follows:

1. **Thermodynamic decoupling and self-lofting:** While the initial trajectory of the ice plume is kinematically governed by the vertical velocity at the injection moment, a decisive transition occurs after approximately 300–500 s. Regardless of whether the plume is seeded into an updraft or a downdraft, it eventually exhibits a mostly coherent net ascent. We attribute this universal lofting to the buoyancy generated by latent heat release from vapor deposition, which overcomes initial subsidence.

2. **Vertical dispersion and detectability trade-off:** The interaction between this induced ascent and the cloud-top inversion creates a trade-off. Plumes in updrafts ascend rapidly but are terminated by the inversion layer ("ceiling effect"). Conversely, plumes in downdrafts traverse the boundary layer more slowly, resulting in a larger vertical dispersion (up to ~ 250 m spread). Crucially, this enhanced vertical dispersion compensates for the lower mean altitude of downdraft plumes, ensuring that the seeding signature remains geometrically detectable by downstream in situ sampling.

3. **Microphysical resilience and transient desiccation:** The size of the ice crystals increases consistently, and the size distribution is similar across all regimes. However, the persistence of the liquid phase is sensitive to the trajectory.

https://doi.org/10.5194/egusphere-2026-470
Preprint. Discussion started: 17 February 2026

Downdraft-seeded plumes exhibit a transient "dip" in liquid water content and relative humidity around $t \approx 200$ s as they approach the drier air below cloud base. Despite this temporary desiccation, the subsequent latent-heat-driven re-ascent allows the plume to recover and remain within the mixed-phase regime.

These findings have significant implications for both observational strategies and numerical modeling of precipitation enhancement. First, the identification of the "self-lofting" mechanism suggests that glaciogenic seeding is more dynamically robust than previously assumed; the success of seeding is not strictly contingent on targeting pre-existing updrafts, as the plume is capable of generating its own buoyancy to sustain its advection time in the mixed-phase layer. Second, the structural analysis confirms that Eulerian observations (e.g., fixed ground sites) are likely to capture the seeding signal, even in downdraft conditions, due to the compensatory effect of enhanced vertical dispersion.

Future work should expand this analysis to include a wider range of environmental conditions. Specifically, it would be interesting to vary the vertical wind shear profiles, as the strength of the shear directly modulates the boundary layer mixing processes and the lateral spreading of the ice plume. Additionally, sensitivity studies regarding thermodynamic profiles, such as temperature and latent water content (LWC), are warranted. These variables directly govern ice crystal habit regimes and riming efficiency, thereby influencing the magnitude of latent heat release.

Furthermore, the updrafts and downdrafts in this idealized framework are generated internally by boundary-layer mixing and therefore have characteristic horizontal scales of approximately $\mathcal{O}(100)$ m. In realistic atmospheric conditions, however, vertical motions in stratiform clouds also include larger-scale components, such as those associated with orographically forced gravity waves and mesoscale circulations. Incorporating vertical motions across a wider range of spatial scales would allow for a more comprehensive assessment of their interactions with smaller-scale motions and the associated microphysical–thermodynamic feedbacks.

Finally, since this study relied on a specific bin microphysics scheme, inter-comparison with bulk microphysics schemes would be valuable to determine whether standard parameterizations can adequately resolve the latent heat feedbacks that drive the secondary plume ascent. Ultimately, recognizing the active thermodynamic role of seeded ice plumes is essential for refining the representation of aerosol-cloud interactions for weather modification simulations.

Code and data availability. Data and scripts will be uploaded into a repository upon acceptance, and are available upon request until then.

Author contributions. U.L. and J.H. conceived the CLOUDLAB project and secured funding. C.O. performed the model simulations, while H.Z. analyzed the observational data from the seeding experiments. H.Z. and C.O. conducted the scientific analysis together. Regarding visualization, C.O. provided the initial data processing code, and H.Z. performed the post-processing and prepared the figures. H.Z. and C.O. wrote the original draft; specifically, C.O. drafted the sections on numerical setup and model validation, while H.Z. wrote the rest of the manuscript. U.L., J.H., and A.D. supervised the study and provided scientific guidance. All authors contributed to the review and editing of the manuscript and approved the final version.

https://doi.org/10.5194/egusphere-2026-470
Preprint. Discussion started: 17 February 2026

Competing interests. The authors declare that they have no conflict of interest.

Acknowledgements. We acknowledge financial support from the European Research Council (ERC) under the European Union's Horizon 2020 research and innovation program (grant no. 101021272), as well as from the EXCLAIM project funded by ETH Zurich. We extend our sincere gratitude to our colleagues at ETH Zurich: Nadja Omanovic for developing the frozen fraction function, and Christopher Fuchs, Fabiola Ramelli, Anna J. Miller, Nadja Omanovic, and Robert Spirig for their assistance with the seeding experiments and in situ measurements. From TROPOS, we thank Patric Seifert for providing the vertically pointing and scanning Doppler cloud radars and Kevin Ohneiser for maintaining the instrumentation. Numerical simulations were performed on the Euler cluster operated by the High Performance Computing group at ETH Zurich. Data analysis and storage resources were provided by the Swiss National Supercomputing Centre (CSCS) in Lugano under project cwd01 (AD).

https://doi.org/10.5194/egusphere-2026-470
Preprint. Discussion started: 17 February 2026

References

Abade, G. C. and Albuquerque, D. G.: Persistent mixed-phase states in adiabatic cloud parcels under idealised conditions, Quarterly Journal of the Royal Meteorological Society, 150, 3450–3474, 2024.

Ansmann, A., Tesche, M., Seifert, P., Althausen, D., Engelmann, R., Fruntke, J., Wandinger, U., Mattis, I., and Müller, D.: Evolution of the ice phase in tropical altocumulus: SAMUM lidar observations over Cape Verde, Journal of Geophysical Research: Atmospheres, 114, 2009.

Bühl, J., Seifert, P., Engelmann, R., and Ansmann, A.: Impact of vertical air motions on ice formation rate in mixed-phase cloud layers, npj Climate and Atmospheric Science, 2, 36, 2019.

Chen, J.-P. and Lamb, D.: The Theoretical Basis for the Parameterization of Ice Crystal Habits: Growth by Vapor Deposition, Journal of Atmospheric Sciences, 51, 1206–1222, 1994.

Fuchs, C., Ramelli, F., Miller, A. J., Omanovic, N., Spirig, R., Zhang, H., Seifert, P., Ohneiser, K., Lohmann, U., and Henneberger, J.: Quantifying ice crystal growth rates in natural clouds from glaciogenic cloud seeding experiments, EGUsphere, 2025, 1–28, 2025.

Grabowski, W. W. and Abade, G. C.: Broadening of Cloud Droplet Spectra through Eddy Hopping: Turbulent Adiabatic Parcel Simulations, Journal of the Atmospheric Sciences, 74, 1485–1493, 2017.

Hashino, T. and Tripoli, G.: The Spectral Ice Habit Prediction System (SHIPS). Part I: Model description and simulation of the vapor deposition process, Journal of the Atmospheric Sciences, 64, 2210–2237, 2007a.

Hashino, T. and Tripoli, G. J.: The Spectral Ice Habit Prediction System (SHIPS). Part I: Model Description and Simulation of the Vapor Deposition Process, Journal of the Atmospheric Sciences, 64, 2210–2237, 2007b.

Hashino, T. and Tripoli, G. J.: The Spectral Ice Habit Prediction System (SHIPS). Part II: Simulation of Nucleation and Depositional Growth of Polycrystals, Journal of the Atmospheric Sciences, 65, 3071–3094, 2008.

Hashino, T. and Tripoli, G. J.: The Spectral Ice Habit Prediction System (SHIPS). Part III: Description of the Ice Particle Model and the Habit-Dependent Aggregation Model, Journal of the Atmospheric Sciences, 68, 1125–1141, 2011.

Henneberger, J., Ramelli, F., Spirig, R., Omanovic, N., Miller, A. J., Fuchs, C., Zhang, H., Bühl, J., Hervo, M., Kanji, Z. A., et al.: Seeding of supercooled low stratus clouds with a UAV to study microphysical ice processes: an introduction to the CLOUDLAB project, Bulletin of the American Meteorological Society, 104, E1962–E1979, 2023.

Korolev, A. and Field, P. R.: The effect of dynamics on mixed-phase clouds: Theoretical considerations, Journal of the Atmospheric Sciences, 65, 66–86, 2008.

Korolev, A., McFarquhar, G., Field, P. R., Franklin, C., Lawson, P., Wang, Z., Williams, E., Abel, S. J., Axisa, D., Borrmann, S., et al.: Mixed-phase clouds: Progress and challenges, Meteorological Monographs, 58, 5–1, 2017.

Korolev, A. V., Isaac, G. A., Cober, S. G., Strapp, J. W., and Hallett, J.: Microphysical characterization of mixed-phase clouds, Quarterly Journal of the Royal Meteorological Society: A journal of the atmospheric sciences, applied meteorology and physical oceanography, 129, 39–65, 2003.

Lilly, D. K.: On the numerical simulation of buoyant convection, Tellus, 14, 148–172, 1962.

Miller, A. J., Ramelli, F., Fuchs, C., Omanovic, N., Spirig, R., Zhang, H., Lohmann, U., Kanji, Z. A., and Henneberger, J.: Two new multirotor uncrewed aerial vehicles (UAVs) for glaciogenic cloud seeding and aerosol measurements within the CLOUDLAB project, Atmospheric Measurement Techniques, 17, 601–625, 2024.

https://doi.org/10.5194/egusphere-2026-470
Preprint. Discussion started: 17 February 2026

Miller, A. J., Fuchs, C., Ramelli, F., Zhang, H., Omanovic, N., Spirig, R., Marcolli, C., Kanji, Z. A., Lohmann, U., and Henneberger, J.: Quantified ice-nucleating ability of AgI-containing seeding particles in natural clouds, Atmospheric Chemistry and Physics, 25, 5387–5407, 2025.

Morrison, H., De Boer, G., Feingold, G., Harrington, J., Shupe, M., and Sulia, K.: Resilience of persistent Arctic mixed-phase clouds, Nat. Geosci., 5, 11–17, 2012.

Nishizawa, S., Yashiro, H., Sato, Y., Miyamoto, Y., and Tomita, H.: Influence of grid aspect ratio on planetary boundary layer turbulence in large-eddy simulations, Geoscientific Model Development, 8, 3393–3419, 2015.

Omanovic, N., Ferrachat, S., Fuchs, C., Henneberger, J., Miller, A. J., Ohneiser, K., Ramelli, F., Seifert, P., Spirig, R., Zhang, H., and Lohmann, U.: Evaluating the Wegener–Bergeron–Findeisen process in ICON in large-eddy mode with in situ observations from the CLOUDLAB project, Atmospheric Chemistry and Physics, 24, 6825–6844, 2024.

Ong, C. R., Koike, M., Hashino, T., and Miura, H.: Modeling Performance of SCALE-AMPS: Simulations of Arctic Mixed-Phase Clouds Observed During SHEBA, Journal of Advances in Modeling Earth Systems, 14, e2021MS002 887, 2022.

Pinsky, M. and Khain, A.: Effects of in-cloud nucleation and turbulence on droplet spectrum formation in cumulus clouds, Quarterly Journal of the Royal Meteorological Society: A journal of the atmospheric sciences, applied meteorology and physical oceanography, 128, 501–533, 2002.

Pruppacher, H. R., Klett, J. D., and Wang, P. K.: Microphysics of clouds and precipitation, 1998.

Ramelli, F., Beck, A., Henneberger, J., and Lohmann, U.: Using a holographic imager on a tethered balloon system for microphysical observations of boundary layer clouds, Atmospheric Measurement Techniques, 13, 925–939, 2020.

Ramelli, F., Henneberger, J., Fuchs, C., Miller, A. J., Omanovic, N., Spirig, R., Zhang, H., David, R. O., Ohneiser, K., Seifert, P., et al.: Repurposing weather modification for cloud research showcased by ice crystal growth, PNAS nexus, 3, pgae402, 2024.

Rauber, R. M. and Tokay, A.: An explanation for the existence of supercooled water at the top of cold clouds, Journal of Atmospheric Sciences, 48, 1005–1023, 1991.

Sato, Y., Nishizawa, S., Yashiro, H., Miyamoto, Y., Kajikawa, Y., and Tomita, H.: Impacts of cloud microphysics on trade wind cumulus: which cloud microphysics processes contribute to the diversity in a large eddy simulation?, Progress in Earth and Planetary Science, 2, 2015.

Scherrer, S. C. and Appenzeller, C.: Fog and low stratus over the Swiss Plateau-a climatological study, International Journal of Climatology, 34, 678–686, 2014.

Sekiguchi, M. and Nakajima, T.: A k-distribution-based radiation code and its computational optimization for an atmospheric general circulation model, Journal of Quantitative Spectroscopy and Radiative Transfer, 109, 2779–2793, 2008.

Shupe, M. D., Kollias, P., Persson, P. O. G., and McFarquhar, G. M.: Vertical motions in Arctic mixed-phase stratiform clouds, Journal of the Atmospheric Sciences, 65, 1304–1322, 2008.

Smagorinsky, J.: General circulation experiments with the primitive equations: I. the basic experiment, Monthly Weather Review, 91, 99–164, 1963.

Touloupas, G., Lauber, A., Henneberger, J., Beck, A., and Lucchi, A.: A convolutional neural network for classifying cloud particles recorded by imaging probes, Atmospheric Measurement Techniques, 13, 2219–2239, 2020.

Westbrook, C. and Illingworth, A.: The formation of ice in a long-lived supercooled layer cloud, Quarterly Journal of the Royal Meteorological Society, 139, 2209–2221, 2013.

https://doi.org/10.5194/egusphere-2026-470
Preprint. Discussion started: 17 February 2026

Zhang, H., Li, X., Ramelli, F., David, R. O., Pasquier, J., and Henneberger, J.: IceDetectNet: A rotated object detection algorithm for classifying components of aggregated ice crystals with a multi-label classification scheme, Atmospheric Measurement Techniques, 17, 7109–7128, 2024.

Zhang, H., Ramelli, F., Fuchs, C., Omanovic, N., Miller, A. J., Spirig, R., Wu, Z., Chu, Y., Li, X., Lohmann, U., et al.: Inferring the Controlling Factors of Ice Aggregation from Targeted Cloud Seeding Experiments, EGUsphere, 2025, 1–31, 2025.